Refined Multi-Phase-Lag Model for Magneto-thermoelastic Interaction with Rotation and Laser Pulse

Amrita De[1], Pallabi Purkait[2], Payel Das[3, *], Mridula Kanoria[4]

[1, 3] *Department of Basic Engineering Sciences and Humanities, Netaji Subhash Engineering College, Kolkata, India*
[2] *Department of Mathematics, Banwarilal Bhalotia College, Asansol, India*
[4] *Department of Mathematics, Sister Nivedita University, Kolkata, India*

Abstract: *This study explores wave propagation in a rotating, two-dimensional magneto-thermoelastic medium heated by a non-Gaussian laser pulse, using the refined multi-phase-lag (MPL) thermoelasticity model with memory-dependent derivatives. It encompasses Lord-Shulman, simple phase-lag, and Green-Naghdi II theories as special cases of MPL model. Laplace and Fourier transforms are applied to derive analytical solutions, with numerical inversion performed by the Zakian method in Mathematica 10. Graphs illustrate the effects of different theories, rotation, and magnetic fields on displacement, temperature, and stress.*

Keywords: *Laser pulse, Rotating Medium, Magnetic field, Refined multi-phase-lag model, Memory dependent derivative, Laplace and Fourier transform technique.*

1. Introduction

Neumann's uncoupled thermoelasticity theory has two major limitations: it lacks an elastic term in the heat conduction equation and predicts infinite heat wave speed due to its parabolic nature. To address this, Biot [1] developed the coupled thermoelasticity theory, which links thermal and elastic effects but still retains the issue of infinite speed of heat propagation. Lord and Shulman [2] later improved upon this by introducing a relaxation time, making the heat conduction equation hyperbolic and ensuring finite propagation speeds for thermal and elastic waves. Their model, part of extended thermoelasticity theory (ETE), replaces Fourier's law with the Maxwell-Cattaneo law. De et al. [3] applied the Lord-Shulman model to study thermal damage in living tissues caused by hyperthermic perfusion.

Following the development of the first generalized theory, numerous researchers have proposed additional generalized models to better interpret and match experimental observations. Zenkour [4] proposed a unified generalized refined multi-phase-lag (RPL) heat transport equation that incorporates and extends all the previously developed theories:

*Corresponding author

$$\left[1+\sum_{m=1}^{M}\frac{\tau_\theta^m}{m!}\frac{\partial^m}{\partial t^m}\right]K\nabla^2 T=\left[\delta+\tau_0\frac{\partial}{\partial t}+\sum_{n=1}^{N}\frac{\tau_q^{n+1}}{(n+1)!}\frac{\partial^{n+1}}{\partial t^{n+1}}\right]\left(\rho c_e\frac{\partial T}{\partial t}+\gamma T_0\frac{\partial e}{\partial t}\right) \qquad (1)$$

Here K means thermal conductivity, T refers to the temperature measured above the baseline temperature T_0, c_e represents the specific heat capacity under constant strain, γ stands for the thermal modulus, ρ means the mass density. According to the applied thermoelasticity theory, the parameter δ takes value either 0 or 1. Also, τ_0 denotes the first relaxation time, τ_q and τ_θ are the phase-lags of the heat flux and of temperature gradient respectively. In the context of the RPL theory, the value of M, N may take values of 5 or more as needed.

This theory encompasses several thermoelastic models including the coupled thermoelasticity theory (CTE), Lord and Shulman's generalized theory (LS), Green and Naghdi type II (GN II), the simple phase lag (SPL), and the refined phase lag (RPL) model by varying the parameters $\tau_q, \tau_\theta, \tau_0$ and δ. The refined model has been widely applied to develop frameworks for various physical phenomena. For instance, Mashat and Zenkour [5] studied nanobeam vibrations, Zenkour [6] explored thermo-diffusion in cylinders, Purkait and Kanoria [7] examined functionally graded materials under gravity, and Bhattacharya and Kanoria [8] investigated elastothermo-diffusive effects with harmonic heat sources.

In recent years, fractional derivatives have gained significant attention across various fields for their ability to model memory effects in physical systems. Diethelm [9] advanced the use of the Caputo derivative [10], which employs a fixed kernel function$k_\beta(t-\xi)$. However, this fixed kernel limits flexibility in capturing a wide range of real-world behaviors. To overcome this limitation, Wang and Li [11] introduced the memory-dependent derivative (MDD), which allows the kernel function on the interval $[t-\tau, t]$ to be freely chosen. This approach enhances the model's ability to represent time-delay and memory effects more accurately. The kernel function $k(t-\xi)$can be chosen freely as follows:

$$
\begin{aligned}
k(t-\xi) &= 1-\frac{2f}{\tau}(t-\xi)+\frac{e^2}{\tau^2}(t-\xi)^2 \\
&= 1 \qquad \text{if } e=f=0 \\
&= 1-\tfrac{t-\xi}{\tau} \qquad \text{if } e=0,\ f=\tfrac{1}{2} \qquad (2) \\
&= \left(1-\frac{t-\xi}{\tau}\right)^2 \qquad \text{if } e=1, f=1
\end{aligned}
$$

Unlike fractional derivatives, memory dependent derivatives (MDD) offer a more intuitive physical interpretation by directly linking the present state to past values through a freely chosen kernel function. This flexibility makes MDD especially suitable for modeling real-world problems in generalized thermoelasticity. Several pioneering studies have further advanced this concept, as noted in the literature [12, 13]. Importantly, MDD reduces to the classical derivative as $\tau \longrightarrow 0$, maintaining consistency with traditional models. Recently, various problems in generalized thermoelasticity using MDD have been explored in studies such as those cited in [14–18].

As a coupled theory, magneto-thermoelasticity integrates magnetic, thermal, and elastic fields, where magnetic behavior is governed by Maxwell's equations. This field has attracted growing interest due to its wide-ranging applications in geophysics, plasma physics and nuclear science. Studying wave propagation in rotating magneto-thermoelastic media is essential for accurately modeling conditions such as the Earth's rotation and magnetic field effects on seismic behavior. Significant contributions in this area have been made by Sur et al. [19], Mondal et al. [20,21], and Purkait et al. [15], particularly regarding the effects of magnetic fields. Many researchers have further explored thermoelastic responses under combined magnetic and rotational influences. Notably, Das and Kanoria [22] investigated finite thermoelastic wave propagation in an unbounded rotating medium subjected to a periodically varying heat source in the presence of a magnetic field.

Pulsed and ultra-short lasers, operating on nanosecond to femtosecond timescales, have attracted considerable interest for generating thermal waves in solids due to their widespread applications in material processing and non-destructive testing. Zenkour et al. [23, 24] and Kutbi et al. [25] explored refined two-temperature and multi-phase-lag theories in thermoelastic media subjected to pulsed laser heating. Additionally, De et al. [26] and Purkait and Kanoria [27] studied the influence of magnetic fields, gravity, and inclined loading on two-dimensional thermoelastic media using generalized and dual phase lag models.

Considering these developments, the present study investigates the impact of rotation and magnetic fields on a two-dimensional thermoelastic medium with memory effects, using the refined multi-phase-lag (MPL) model, which encompasses several existing theories. Analytical expressions for displacement, stress, and temperature under pulsed laser heating are obtained using Laplace and Fourier transforms, with numerical inversion of the double transform carried out in MATHEMATICA 10. The Zakian method [28] is employed for the numerical inversion of the Laplace transform. Graphical results are presented to compare the refined model with other established thermoelastic theories.

2. Formulation of the problem

The medium under consideration is homogeneous, isotropic, and perfectly conducting, and it is exposed to a constant magnetic field oriented along the z-axis, $H = (0, 0, H_0)$. This medium undergoes uniform rotation with angular velocity $\Omega = \Omega n$, where n is a unit vector aligned with the axis of rotation (as illustrated in Figure 1). In the rotating frame of reference, a fixed coordinate system is assumed within the rotating medium, the equation of motion includes two additional terms: the centripetal acceleration $\Omega \times (\Omega \times u)$, which accounts for time-varying motion, and the Coriolis acceleration $2\Omega \times \dot{u}$.

For a two-dimensional problem, we consider u and v as the dynamic displacement components in the x and y directions, respectively, and T as the temperature distribution.

These variables are represented as:

$$u = u(x, y, t), \qquad v = v(x, y, t), \qquad T = T(x, y, t)$$

When free charge density and displacement current are absent, the behavior of the electromagnetic field is governed by the simplified form of Maxwell’s equations, given as:

$$\nabla \times h = J + \epsilon_0 \frac{\partial E}{\partial t} \quad (3) \qquad \nabla \times E = -\mu_0 \frac{\partial h}{\partial t} \quad (4)$$

$$E = -\mu_0 \left(\frac{\partial u}{\partial t} \times H \right) \quad (5) \qquad \nabla . h = 0, \nabla . E = 0 \quad (6)$$

where $h = (0, 0, h_0)$ denotes induced magnetic field, ϵ_0 represents electric permittivity, μ_0 means magnetic permeability, E is the induced electric field, $E = (E_1, E_2, 0)$, J denotes conduction current density and $H(= H_0 + h)$ represents total magnetic field.

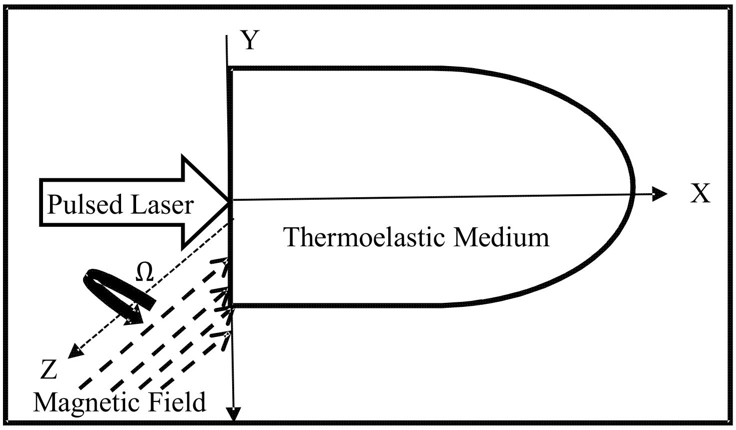

Figure 1. Geometry of the problem

The stress-displacement-temperature relations are expressed as follows:

$$\sigma_{xx} = (\lambda + 2\mu)\frac{\partial u}{\partial x} + \lambda\frac{\partial v}{\partial y} - \gamma(T - T_0) \quad (7) \quad \sigma_{yy} = (\lambda + 2\mu)\frac{\partial v}{\partial y} + \lambda\frac{\partial u}{\partial x} - \gamma(T - T_0) \quad (8)$$

$$\sigma_{xy} = \mu\left(\frac{\partial u}{\partial y} + \frac{\partial v}{\partial x}\right) \quad (9)$$

where λ, μ are the Lame' constants, T is the temperature measured above the baseline temperature T_0 and $\gamma = (3\lambda + 2\mu)\alpha_t$, α_t is the coefficient of linear thermal expansion.
The strain-displacement relations are given by: $e_{ij} = \frac{1}{2}\left(u_{i,j} + u_{j,i}\right)$

In the presence of Lorentz forces, the equations of motion can be written as:

$$(\lambda + 2\mu + \mu_0 H_0^2)\frac{\partial^2 u}{\partial x^2} + (\lambda + \mu + \mu_0 H_0^2)\frac{\partial^2 v}{\partial x \partial y} - \gamma\frac{\partial \mathrm{T}}{\partial \mathrm{x}} + \mu\frac{\partial^2 u}{\partial y^2} = \rho\left[\frac{\partial^2 u}{\partial t^2} - \Omega^2 u - 2\Omega\frac{\partial v}{\partial \mathrm{t}}\right] \quad (10)$$

$$(\lambda + 2\mu + \mu_0 H_0^2)\frac{\partial^2 v}{\partial y^2} + (\lambda + \mu + \mu_0 H_0^2)\frac{\partial^2 u}{\partial x \partial y} - \gamma\frac{\partial \mathrm{T}}{\partial \mathrm{y}} + \mu\frac{\partial^2 v}{\partial x^2} = \rho\left[\frac{\partial^2 v}{\partial t^2} - \Omega^2 v + 2\Omega\frac{\partial u}{\partial \mathrm{t}}\right] \quad (11)$$

where $\mu_0 H_0^2\left(\frac{\partial^2 u}{\partial x^2} + \frac{\partial^2 v}{\partial x \partial y}\right)$, $\mu_0 H_0^2\left(\frac{\partial^2 u}{\partial x \partial y} + \frac{\partial^2 v}{\partial y^2}\right)$ are Lorentz force's components.

Within the framework of memory dependent derivative (MDD), the heat conduction equation in the RPL model, considering the presence of a heat source Q, is expressed as follows:

$$\left[1 + \sum_{m=1}^{M}\frac{\tau_\theta^m}{m!}D_{\tau_\theta}^m\right]K\nabla^2 T = \left[\delta + \tau_0 D_{\tau_0} + \sum_{n=1}^{N}\frac{\tau_q^{n+1}}{(n+1)!}D_{\tau_q}^{n+1}\right]\left(\rho c_e\frac{\partial T}{\partial t} + \gamma T_0\frac{\partial e}{\partial t} - \rho Q\right) \quad (12)$$

Depending on the values of $\tau_q, \tau_\theta, \tau_0, \delta, M$ and N, Eq. (12) simplifies to the heat conduction equation of CTE, LS theory, GN II model, SPL and RPL theory incorporating memory dependent derivative.

For convenience, the following non-dimensional quantities are introduced:

$$(x', y', u', v') = C_0\eta_0(x, y, u, v), \quad (t', \tau') = C_0^2\eta_0(t, \tau), \quad \Omega' = \frac{\Omega}{C_0^2\eta_0}, \quad \eta_0 = \frac{\rho C_E}{K}$$

$$\sigma'_{ij} = \frac{\sigma_{ij}}{\mu}, C_0^2 = \frac{\lambda + 2\mu}{\rho}, \quad \theta' = \frac{\gamma(T - T_0)}{\lambda + 2\mu}, \quad Q' = \frac{\gamma}{C_E C_0^2\eta_0(\lambda + 2\mu)}Q, \quad \epsilon = \frac{\gamma^2 T}{K\eta_0(\lambda + 2\mu)} \tag{13}$$

Removing the dashes for convenience and using the quantities stated in Eq. (13), Eqs. (10-12) reduced to the non-dimensional form as follows:

$$[(\beta^2 - 1) + R_H\beta^2]\frac{\partial e}{\partial x} + \nabla^2 u - \beta^2\frac{\partial \theta}{\partial x} = \beta^2\left[\frac{\partial^2 u}{\partial t^2} - \Omega^2 u - 2\Omega\frac{\partial \mathrm{v}}{\partial \mathrm{t}}\right] \tag{14}$$

$$[(\beta^2 - 1) + R_H\beta^2]\frac{\partial e}{\partial y} + \nabla^2 v - \beta^2\frac{\partial \theta}{\partial y} = \beta^2\left[\frac{\partial^2 v}{\partial t^2} - \Omega^2 v + 2\Omega\frac{\partial \mathrm{u}}{\partial \mathrm{t}}\right] \tag{15}$$

And $\left[1 + \sum_{m=1}^{M}\frac{\tau_\theta^m}{m!}D_{\tau_\theta}^m\right]\nabla^2\theta = \left[\delta + \tau_0 D_{\tau_0} + \sum_{n=1}^{N}\frac{\tau_q^{n+1}}{(n+1)!}D_{\tau_q}^{n+1}\right]\left(\dot{\theta} + \epsilon\dot{e} - Q\right)$ (16)

Also the stress components become:

$$\sigma_{xx} = 2\frac{\partial u}{\partial x} + (\beta^2 - 2)e - \beta^2\theta \tag{17}$$

$$\sigma_{yy} = 2\frac{\partial v}{\partial y} + (\beta^2 - 2)e - \beta^2\theta \tag{18}$$

$$\sigma_{xy} = \left(\frac{\partial u}{\partial y} + \frac{\partial v}{\partial x}\right) \tag{19}$$

Also $\quad e = \frac{\partial \mathrm{u}}{\partial \mathrm{x}} + \frac{\partial \mathrm{v}}{\partial \mathrm{y}}$ (20)

Now in Eq. (16),

(I) $\tau_q = \tau_\theta = \tau_0 = 0$ and $\delta = 1$, yields the heat conduction of CTE theory based on MDD.

(II) $\delta = 1, \tau_q, \tau_\theta \to 0$ and $\tau_0 > 0$, yields the heat conduction of L-S theory based on MDD.

(III) $\tau_q, \tau_\theta \to 0$, $\delta = 0$ and $\tau_0 = 1$, yields the heat conduction of G-N(II) theory based on MDD.

(IV) $\tau_q = \tau_0, \tau_\theta \geq 0, \delta = 1, N = 1$ and $\tau_q^2 = 0$, yields heat conduction of SPL based on MDD.

(V) $\tau_q = \tau_0 > \tau_\theta \geq 0, \delta = 1$ and $N \geq 1$, yields the heat conduction of RPL based on MDD.

To neglect the effects of centrifugal stiffening, a low speed assumption is adopted in the subsequent analysis. Now from Eq. (14) and Eq. (15) we get

$$\left[(1 + R_H)\nabla^2 - \frac{\partial^2}{\partial t^2} + \Omega^2\right]e = \nabla^2\theta + 2\Omega\frac{\partial \zeta}{\partial \mathrm{t}} \tag{21}$$

$$\left[\nabla^2 - \beta^2\left(\frac{\partial^2}{\partial t^2} - \Omega^2\right)\right]\zeta = -2\Omega\beta^2\frac{\partial \mathrm{e}}{\partial \mathrm{t}} \tag{22}$$

where $\beta^2 = \frac{(\lambda+2\mu)}{\mu}$, $\nabla^2 = \frac{\partial^2}{\partial x^2} + \frac{\partial^2}{\partial y^2}$ is Laplace's operator in two-dimensional space.

Also, $\quad \zeta = \frac{\partial u}{\partial y} - \frac{\partial v}{\partial x}$ (23)

The laser-induced heat input is mathematically represented as follows [29]

$$Q = \frac{I_0\gamma_1}{2\pi r^2} e^{\left(-\frac{y^2}{r^2} - \gamma_1 x\right)} f(t) \tag{24}$$

where I_0 means laser intensity, r represents beam radius and γ_1 characterizes the depth at which the laser energy is absorbed.
The definition of temporal profile $f(t)$ is as follows:

$$f(t) = \frac{t}{t_0^2} e^{-\frac{t}{t_0}} \tag{25}$$

where t_0 denotes the time interval over which the laser pulse is applied.
The initial conditions are: $u = \dot{u} = v = \dot{v} = \theta = \dot{\theta} = 0$
The boundary condition on $x = 0$are given by

$$\sigma_{xx}(0, y, t) = \sigma_{xy}(0, y, t) = 0; \;\; \theta(0, y, t) = H(r - |y|)e^{-bt} \tag{26}$$

3. Method of solution

Applying Laplace transformation defined as

$$\bar{f}(x, y, s) = \mathcal{L}[f(x, y, t)] = \int_0^\infty f(x, y, t)e^{-st}\, dt, \quad Re(s) > 0 \tag{27}$$

to the memory-dependent derivative operator D_τ^m and using the convolution theorem, we get,

$$\mathcal{L}[\tau_0 D_\tau^m f(t)] = \mathcal{L}\left[\int_{t-\tau_0}^{t} K(t-\xi) f^m(\xi) d\xi\right] = s^{m-1} G_\omega(s, \tau_0)\mathcal{L}(f(t)) \tag{28}$$

Depending on the choice of the kernel function$K(t - \xi)$, in Eq. (2) of the introduction, we obtain the following

$$G_\omega(s) = 1 - \frac{2f}{\omega s} + \frac{2e^2}{\omega^2 s^2} - e^{-\omega s}\left[(1 - 2f + e^2) + \frac{2(e^2 - f)}{\omega s} + \frac{2e^2}{\omega^2 s^2}\right]$$

The Fourier transformation with respect to y defined by

$$\hat{\bar{f}}(x, \xi, s) = \mathcal{F}[\bar{f}(x, y, s)] = \int_{-\infty}^{\infty} \bar{f}(x, y, s)e^{-i\xi y}\, dy, \quad i = \sqrt{-1}$$

On taking Laplace and Fourier double transformation, Eqs. (16), (21) and (22) reduce to

$$(a_{11}D^2 - a_2)\hat{\bar{\theta}} - a_3\hat{\bar{e}} = a_4 Q_0 e^{-\gamma_1 x} \tag{29}$$

$$(a_5 D^2 - a_6)\hat{\bar{e}} - (D^2 - a_7)\hat{\bar{\theta}} - a_8\hat{\bar{\zeta}} = 0 \tag{30}$$

$$(D^2 - a_9)\hat{\bar{\zeta}} - a_{10}\hat{\bar{e}} = 0 \tag{31}$$

where$D = \frac{d}{dy}$, $Q_0 = \frac{I_0\gamma_1}{2\sqrt{\pi} r(1+st_0)^2} e^{-\frac{r^2\xi^2}{4}}$ and

$a_2 = \xi^2\left(1 + \sum_{m=1}^{M} \frac{\tau_\theta^{m-1}}{m!} s^{m-1} G_\omega\right) - \left(\delta + G_\omega + \sum_{n=1}^{N} \frac{\tau_q^n}{(n+1)!} G_\omega s^n\right) s,$

$a_3 = \left(\delta + G_\omega + \sum_{n=1}^{N} \frac{\tau_q^n}{(n+1)!} G_\omega s^n\right) s\epsilon,$ $\quad a_4 = -\left(\delta + G_\omega + \sum_{n=1}^{N} \frac{\tau_q^n}{(n+1)!} G_\omega s^n\right),$

$a_5 = 1 + R_H,$ $\quad a_6 = \xi^2(1 + R_H) + s^2 - \Omega^2,$ $\quad a_7 = \xi^2,$ $\quad a_8 = 2\Omega s,$

$$a_9 = \xi^2 + \beta^2(s^2 - \Omega^2), \qquad a_{10} = -2\Omega\beta^2 s, \qquad a_{11} = 1 + \sum_{m=1}^{M} \frac{\tau_\theta^{m-1}}{m!} s^{m-1} G_\omega$$

The transformed temperature $\hat{\bar{\theta}}$ satisfies the following sixth-order ordinary differential equation by eliminating $\hat{\bar{e}}$ and $\hat{\bar{\zeta}}$ between Eqs. (29) - (31):

$$(D^6 - AD^4 + BD^2 - C)\hat{\bar{\theta}} = \frac{1}{a_5 a_{11}}[a_4 a_5 \gamma_1^4 - (a_4 a_5 a_9 + a_4 a_6)\gamma_1^2 + (a_4 a_6 a_9 - a_4 a_8 a_{10})]Q_0 e^{-\gamma_1 x} \qquad (32)$$

where

$$A = \frac{a_2 a_5 + a_5 a_9 + a_6 + a_3}{a_5 a_{11}},$$

$$B = \frac{a_2 a_5 a_9 + a_2 a_6 + a_6 a_9 - a_8 a_{10} + a_3 a_9 + a_3 a_7}{a_5 a_{11}},$$

$$C = \frac{a_2 a_6 a_9 - a_2 a_8 a_{10} + a_3 a_7 a_9}{a_5 a_{11}}$$

By solving Eq. (32) under the condition that $\hat{\bar{\theta}} \to \infty$ as $x \to \infty$,we get,

$$\hat{\bar{\theta}} = \sum_{j=1}^{3} R_j e^{-k_j x} + L_1 Q_0 e^{-\gamma_1 x} \qquad (33)$$

Where k_j's ($j = 1,2,3$) are the roots with positive real part of the characteristic equation corresponding to Eq. (32), R_j's ($j = 1,2,3$) represents the arbitrary constants,

$L_1 = \frac{a_4 a_5 \gamma_1^4 - (a_4 a_5 a_9 + a_4 a_6)\gamma_1^2 + (a_4 a_6 a_9 - a_4 a_8 a_{10})}{a_5 a_{11} p}$ and $p = \gamma_1^6 - A\gamma_1^4 + B\gamma_1^2 - C$

Substituting Eq. (33) in Eq. (29) we obtain

$$\hat{\bar{e}} = \sum_{j=1}^{3} R_j H_{1j} e^{-k_j x} + L_2 Q_0 e^{-\gamma_1 x} \qquad (34)$$

and again applying Eq. (34) in Eq. (31) we derive,

$$\hat{\bar{\zeta}} = \sum_{j=1}^{3} R_j H_{2j} e^{-k_j x} + L_3 Q_0 e^{-\gamma_1 x} \qquad (35)$$

Where $H_{1j} = \frac{a_{11}k_j^2 - a_2}{a_3}$, $H_{2j} = \frac{a_{11}(a_{11}k_j^2 - a_2)}{a_3(k_j^2 - a_9)}$, $L_2 = \frac{a_{11}L_1\gamma_1^2 - L_1 a_2 - a_4}{a_3}$, $L_3 = \frac{a_{10}(a_{11}L_1\gamma_1^2 - L_1 a_2 - a_4)}{a_3(\gamma_1^2 - a_9)}$

Then using the result of Eq. (34) in Eq. (20) we obtain,

$$\hat{\bar{u}} = \sum_{j=1}^{3} R_j H_{3j} e^{-k_j x} + L_4 Q_0 e^{-\gamma_1 x} \qquad (36)$$

and substituting Eq. (36) in Eq. (23) we derive,

$$\hat{\bar{v}} = \sum_{j=1}^{3} R_j H_{4j} e^{-k_j x} + L_5 Q_0 e^{-\gamma_1 x} \qquad (37)$$

Where $H_{3j} = \frac{-k_j H_{1j} - i\xi H_{2j}}{k_j^2 - \xi^2}$, $H_{4j} = \frac{k_j H_{2j} + i\xi H_{1j}}{k_j^2 - \xi^2}$, $L_4 = -\frac{L_2\gamma_1 + i\xi L_3}{\gamma_1^2 - \xi^2}$, $L_4 = \frac{L_3\gamma_1 + i\xi L_2}{\gamma_1^2 - \xi^2}$

Upon substituting $\hat{\bar{e}}, \hat{\bar{\theta}}, \hat{\bar{u}}$ and $\hat{\bar{v}}$, into Eqs. (17) - (19) we get

$$\hat{\bar{\sigma}}_{xx} = \sum_{j=1}^{3} R_j H_{5j}\, e^{-k_j x} + L_6 Q_0 e^{-\gamma_1 x} \tag{38}$$

$$\hat{\bar{\sigma}}_{yy} = \sum_{j=1}^{3} R_j H_{6j}\, e^{-k_j x} + L_7 Q_0 e^{-\gamma_1 x} \tag{39}$$

$$\hat{\bar{\sigma}}_{xy} = \sum_{j=1}^{3} R_j H_{7j}\, e^{-k_j x} + L_8 Q_0 e^{-\gamma_1 x} \tag{40}$$

Where $H_{5j} = -2k_j H_{3j} + (\beta^2 - 2)H_{1j} - \beta^2$, $L_6 = -2L_4\gamma_1 + (\beta^2 - 2)L_2 - \beta^2 L_1$
$H_{6j} = (\beta^2 - 2)H_{1j} - 2i\xi H_{4j} - \beta^2$, $L_7 = (\beta^2 - 2)L_2 - 2i\xi L_5 - \beta^2 L_1$
$H_{7j} = -k_j H_{4j} - i\xi H_{3j}$, $L_8 = -\gamma_1 L_5 - i\xi L_4$

Applying the boundary conditions specified in Eq. (26), Eqs. (33), (38), and (40) are modified as follows:

$$\sum R_j e^{-k_j x} + L_1 Q_0 e^{-\gamma_1 x} = \sqrt{\frac{2}{\pi}} \frac{\sin(qr)}{q(s+b)} \tag{41}$$

$$\sum_{j=1}^{3} R_j H_{5j}\, e^{-k_j x} + L_6 Q_0 e^{-\gamma_1 x} = 0 \tag{42}$$

$$\sum_{j=1}^{3} R_j H_{7j}\, e^{-k_j x} + L_8 Q_0 e^{-\gamma_1 x} = 0 \tag{43}$$

The unknown parametersR_j's ($j = 1,2,3$) can be obtained by solving Eqs. (41) - (43).

4. Validity of the Model

To validate the derived equations and results, a comparison is made with the existing study conducted by Othman and Mondal [30]. Their work explores the influence of memory-dependent derivatives in a two-dimensional rotating medium in the context of the Lord–Shulman generalized thermoelasticity theory. Accordingly, in this present problem, when the magnetic field is neglected, the governing equations reduce to those obtained by Othman and Mondal [30] under the specific conditions $\delta = 1, \tau_q = \tau_\theta = 0, Q = 0$. This equivalence can be established analytically as follows.

By imposing $R_H = 0$, the dimensionless form of the equations of motion is derived from Eqs. (14) and (15), which then simplify to:

$$(\beta^2 - 1)\frac{\partial e}{\partial x} + \nabla^2 u - \beta^2 \frac{\partial \theta}{\partial x} = \beta^2 \left[\frac{\partial^2 u}{\partial t^2} - \Omega^2 u - 2\Omega \frac{\partial \mathrm{v}}{\partial \mathrm{t}}\right] \tag{44}$$

$$(\beta^2 - 1)\frac{\partial e}{\partial y} + \nabla^2 v - \beta^2 \frac{\partial \theta}{\partial y} = \beta^2 \left[\frac{\partial^2 v}{\partial t^2} - \Omega^2 v + 2\Omega \frac{\partial \mathrm{u}}{\partial \mathrm{t}}\right] \tag{45}$$

The stress components derived in this study closely resemble those reported by Othman and Mondal [30].

The heat conduction equation can be obtained from Eqs. (16) by setting $\delta = 0, \tau_q = \tau_\theta = 0, \tau_0 = \tau$, eliminating the heat source and neglecting the magnetic field. Under these conditions, Eq. (16) reduces to

$$\nabla^2\theta = (1+\tau D_\tau)(\dot{\theta}+\epsilon\dot{e}) \tag{46}$$

Equations (44), (45) and (46) are identical with the equations (33) and (34) respectively of Othman and Mondal [30].

5. Numerical Result and Discussion

The expressions for displacements, stresses, and temperature distributions are obtained in the transformed domain as $\hat{\hat{f}}(x,\xi,s)$. The inverse Fourier transform is carried out numerically, while the inverse Laplace transform is performed using the Zakian method. For numerical analysis, magnesium has been selected as the material, following the work of Dhaliwal and Singh [31]. All parameter values used in the calculations are expressed in SI units. The constants employed in this study are listed as follows:

$$K = 1.7\times 10^2\,\mathrm{N/K\,sec},\ \ \alpha_T = 1.78\times 10^{-5}K^{-1},\ \ C_E = 1.04\times 10^3\,\mathrm{m^2/K},$$

$$\mu = 3.278\times 10^{10}\,\mathrm{N/m^2},\quad \lambda = 2.17\times 10^{10}\,\mathrm{N/m^2},\ \ I_0 = 10^2\,\mathrm{J/m^2}$$

$$\rho = 1.74\times 10^3\,\mathrm{kg/m^3},\quad \omega = 0.1\mathrm{sec}^{-1},\quad T_0 = 293\mathrm{K}$$

$$r = 0.2\mu\mathrm{m},\quad t = 0.9,\quad \gamma_1 = 25/\mathrm{m},\quad r_1 = 1$$

Table 1 represents a comparison of u, σ_{xx} and σ_{xy} for different values of M and N taking $x = 0.5, t = 0.9, e = f = 1, H_0 = 10^4$ and Ω=1 in case of RPL model. Now if $M = N = 5$ and $M = N = 6$ accuracy up to 5th decimal places is observed from the table.

Table 1: **Distribution of u, σ_{xx} and σ_{xy} for Different Values of M and N**

RPL	u	σ_{xx}	σ_{xy}
M=N=1	−0.335043	6.06567	−2.17428
M=N=2	−0.339565	6.15785	−2.19029
M=N=3	−0.34152	6.18514	−2.20038
M=N=4	−0.34164	6.20935	−2.20421
M=N=5	−0.34165	6.29814	−2.20442
M=N=6	−0.34165	6.29814	−2.20442

The displacement components u, v temperature T and the stress components σ_{xx}, σ_{xy} distributions were evaluated on the x-axis. The computations are performed for four different theories: RPL $(\delta = 1, \tau_\theta = 0.01, \tau_0 = \tau_q = 0.02, M = 7, N = 7)$, SPL $(\delta = 1, \tau_\theta = 0.01, \tau_0 = \tau_q = 0.02,\ \tau_q^2 = 0,\ M = 1)$, LS model $(\delta = 1, \tau_\theta = \tau_q = 0, \tau_0 = 0.01,\ M = 1)$ and GN-II model (δ$= 0, \tau_\theta = \tau_q = 0, \tau_0 = 1$).

Figure 2-6 are plotted to show the impact of four models (RPL, SPL, LS and GN-II) on all physical quantities $I_0 = 10^2$ with respect to kernel functions $k(t - \xi_1) = \left(1 - \frac{t-\xi_1}{\omega}\right)^2$ at a fixed time $t = 0.9$when the magnetic field is present for the rotating medium ($\Omega = 1.0$). The delay time $\omega = 0.1$ and depth $y = 1.0$ are considered for all the figures 2-6.

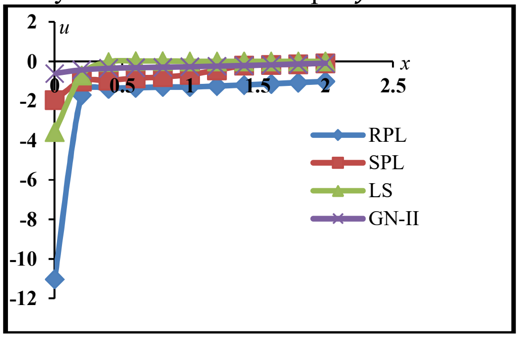

Figure 2. Distribution of u vs. x

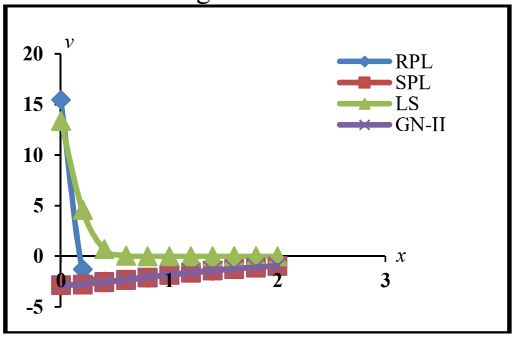

Figure 3. Distribution of v vs. x

Figure 2 illustrates the distribution of horizontal displacement u with respect to distance x. The results show that the displacement remains compressive across all considered models (RPL, SPL, LS, and GN-II), with the maximum values occurring near the boundary. Among them, the RPL model consistently exhibits the highest displacement throughout the domain. Furthermore, for $x < 0.23$, the displacement magnitude follows the order: LS > SPL > GN-II. However, beyond $x = 0.23$, this order changes to SPL > GN-II > LS, while still maintaining compressive behavior. Ultimately, the displacement magnitude diminishes to zero for all models.

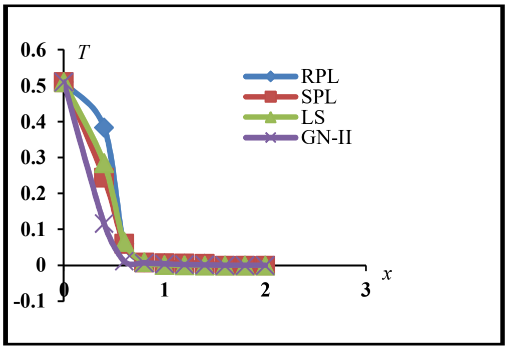

Figure 4. Distribution of T *vs.* x

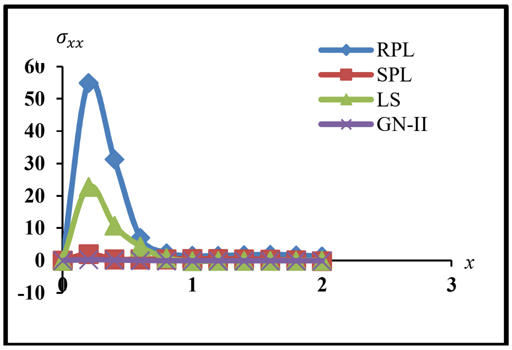

Figure 5. Distribution of σ_{xx} *vs.* x

Figure 3 shows the behavior of vertical displacement v with respect to distance x. For both the RPL and LS models, the displacement v attains its peak at $x = 0$ and gradually decreases to zero. In the RPL model, v remains positive within the range $0 \le x \le 0.16$ and becomes negative for $0.16 \le x \le 0.30$. In contrast, for the LS model, v stays positive up to $x = 0.6$. Meanwhile, the SPL and GN-II models exhibit compressive vertical displacement (negative values) in the range $x = 0$ to $x = 0.3$, after which the displacement vanishes.

Figure 4 depicts the temperature distribution T as a function of distance x. In all cases, the temperature reaches its maximum at $x = 0$, corresponding to the location of thermal shock application, and subsequently decreases with increasing distance. The RPL model exhibits the highest temperature values up to $x = 0.6$, beyond which the temperature profiles for the RPL, SPL, and LS models converge and diminish, approaching zero near $x = 0.8$. In contrast, the GN-II model displays a more rapid temperature decay, with the profile vanishing shortly after $x = 0.6$.

Figure 5 represents the behavior of normal stress σ_{xx} with respect to spatial coordinate x. Across all four models, σ_{xx} increases up to $x = 0.22$, after which it gradually decreases to zero. Among them, the RPL model shows a slower rate of decay compared to the other models, a behavior that is expected due to the inclusion of multiple phase lags, which introduce a delayed thermal response and lead to a more gradual dissipation of thermal energy. Additionally, the RPL model yields the highest values of σ_{xx}, followed by the LS model, then the SPL model, and finally the GN-II model, which exhibits the lowest stress values.

Figure 6 illustrates the behavior of shear stress σ_{xy} with respect to distance x. The shear stress exhibits compressive behavior across all models. Notably, the RPL model demonstrates a significantly higher magnitude of σ_{xy} compared to the other three models. For the RPL model, the shear stress magnitude increases within the range $0 \leq x \leq 0.2$, then gradually decreases and eventually approaches zero. In the case of the LS, SPL, and GN-II models, σ_{xy} also remains compressive throughout, diminishing steadily to zero.

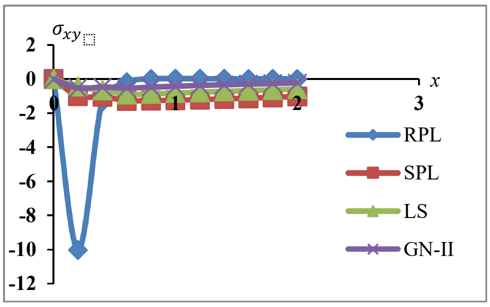

Figure 6. Distribution σ_{xy} vs. x

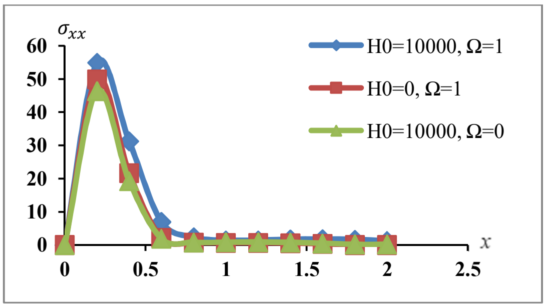

Figure 7. Distribution σ_{xx} vs. x

Figures 7 and 8 are presented to investigate the influence of magnetic field and rotation on the distribution of normal and shear stresses along the x-axis within the framework of the RPL model. The analysis is carried out for an intensity $I_0 = 10^2$, using the kernel function $k(t - \xi_1) = \left(1 - \frac{t-\xi_1}{\omega}\right)^2$, at a fixed time $t = 0.9$. In both figures, the delay time is set as $\omega = 0.1$, and the material depth is taken as $y = 1.0$.

Figure 7 illustrates the behavior of normal stress σ_{xx} along the x-axis. In all scenarios, σ_{xx} increases within the range $0 \leq x \leq 0.22$, then decreases to zero, consistent with the mechanical boundary conditions of the problem. It is also observed that the magnitude of σ_{xx} is greater when the magnetic field strength is H_0 =10000 compared to $H_0 = 0$for the rotating medium with $\Omega = 1.0$. Furthermore, for H_0 =10000, the stress magnitude is higher in the rotating case ($\Omega = 1.0$) than in the non-rotating case ($\Omega = 0$).

Figure 8 shows the variation of shear stress σ_{xy} with respect to x. The stress remains compressive in all cases, with the highest magnitude observed for H_0 =10000 and $\Omega = 1$. The shear stress increases up to $x = 0.20$, then gradually decreases and reaches zero, satisfying the boundary conditions. The figure also demonstrates that for H_0 =10000, the shear stress profile is more pronounced in the rotating medium ($\Omega = 1.0$) compared to the non-rotating case ($\Omega = 0.0$).

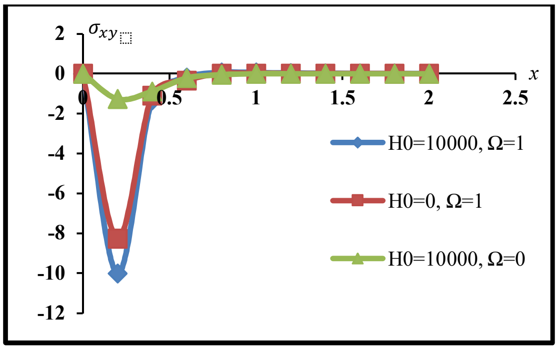

Figure 8. Distribution σ_{xy} vs. x

5. Conclusion.

This study aims to examine how rotation and magnetic fields affect the behavior of physical quantities in memory-dependent generalized thermoelastic wave propagation, employing the RPL model within a two-dimensional rotating medium. While the graphical results effectively highlight several distinct and non-intuitive features that emerge during wave propagation, the following significant observations may be additionally noted:

1. The distributions of displacements and stresses are notably affected by the presence of a magnetic field in a rotating medium. Under the kernel function $K(t-\xi_1) = (1-\frac{t-\xi_1}{\omega})^2$, these physical quantities exhibit an increasing trend with the strength of the magnetic field. Additionally, it is observed that all displacement components diminish and ultimately vanish beyond $x = 0.6$.
2. The choice of kernel function has a significant impact on the results. Specifically, the magnitudes of horizontal displacement u and temperature T are greater when using the kernel $K(t-\xi_1) = (1-\frac{t-\xi_1}{\omega})^2$ compared to the constant kernel $K(t-\xi_1) = 1$. Furthermore, for the $K(t-\xi_1) = (1-\frac{t-\xi_1}{\omega})^2$, the vertical displacement v exhibits both positive and negative values, indicating oscillatory behavior.
3. The magnetic field has no effect on the temperature distribution, as the magnetic and thermal fields are independent in this model.
4. The magnitudes of the displacements u and v are greater in a rotating medium compared to a non-rotating one, for both kernel functions $K(t-\xi_1) = 1$ and $K(t-\xi_1) = 1, (1-\frac{t-\xi_1}{\omega})^2$, in presence of magnetic field.

5. For kernel function $K(t-\xi_1) = (1 - \frac{t-\xi_1}{\omega})^2$, the shear stress exhibits a compressive nature in the rotating medium, while the normal stress shows compressive behavior in the non-rotating medium.

REFERENCES

[1] M. A. Biot, "Thermoelasticity and Irreversible Thermodynamics", *J. Appl. Phys.*, *vol.* ***27****, (1956), pp. 240-253.*

[2] H. W. Lord and Y. A. Shulman, "Generalized dynamical theory of thermoelasticity", *J. Mech. Phys. Solids*, *vol.* ***15****, (1967), pp. 299-309.*

[3] A. De, P. Das and M. Kanoria, "Thermal damages of living tissues due to hyperthermic perfusion", *IJAAMM.*, *vol.* ***9****, No. 4, (2022), pp. 1-11.*

[4] A. M. Zenkour, "Magneto-thermal shock for a fiber-reinforced anisotropic half-space studied with a refined multi-dual-phase-lag model", *J. Phys. Chem. Sol.*, vol. **137**, (2020), *pp.* 109213.

[5] D. S. Mashat and A.M. Zenkour, "Modified DPL Green-Naghdi theory for thermoelastic vibration of temperature-dependent nanobeams", *Results Phys.*, *vol.* ***16****, (2020), pp. 102845.*

[6] A.M. Zenkour, "Thermo-diffusion of solid cylinders based upon refined dual-phase-lag models", *Multidiscip. Model. Mater*, *vol.* ***16****, (2020), pp. 1417-1434.*

[7] P. Purkait and M. Kanoria, "Thermoelastic Interaction in a Functionally Graded Medium Due to Refined Three-Phase-Lag Green-Naghdi Model under Gravitational Field", *Journal of Multiscale Modelling*, *vol.* ***14****, No. 4, (2023), pp. 2350012-309.*

[8] D. Bhattacharya and M. Kanoria, "Refined four-phase lag model for elasto-thermodiffusive interaction with harmonically varying heat sources", *Mechanics of Time-Dependent Materials*, *vol.* ***28****, (2024), pp. 1853-1872.*

[9] K. Diethelm, "The analysis of fractional differential equations: An application-oriented exposition using differential operators of Caputo type", *Springer Science and Business Media*, *(2010).*

[10] M. Caputo, "Linear models of dissipation whose Q is almost frequency independent II", *GJI.*, *vol.* ***13****, (1967), pp. 529-539.*

[11] J. L. Wang and H.F. Li, "Surpassing the fractional derivative: Concept of the memory-dependent derivative. Comput", *Math. with Appl.*, *vol.* ***62****, No. 3, (2011), pp.1562-1567.*

[12] D. Bhattacharya and M. Kanoria, "Modeling the magneto-thermoelastic diffusion in four-phase-lags memory dependent heat transfer", *Mechanics of Time-Dependent Materials*, *vol.* ***28,*** *(2024), pp. 1617-1638.*

[13] S. Mondal, A. Sur and M. Kanoria, "Transient response in a piezoelastic due to the influence of magnetic field with memory dependent derivative", *Acta Mech., vol.* ***230****, (2019), pp. 2325-2338.*

[14] P. Purkait, A. Sur and M. Kanoria, "Elasto-thermodiffusive response in a spherical shell subjected to memory-dependent heat transfer", *Waves in Random and Complex Media*, *vol.* ***31,*** *No. 3, (2019), pp. 515-537.*

[15] P. Purkait, A. Sur and M. Kanoria, "Magneto-thermoelastic interaction in a functionally graded medium under gravitational field", *Waves in Random and Complex Media*, *vol.* ***31****, No. 6, (2019), pp. 1633-1654.*

[16] A. Sur, S. Paul and M. Kanoria, "Modeling of memory-dependent derivative in a functionally graded plate", *Waves in Random and Complex Media*, *vol.* ***31****, No. 4, (2019), pp. 618-638.*

[17] A. Sur and M. Kanoria, "Memory response on thermal wave propagation in an elastic solid with voids", *Mech.*, *vol.* ***48****, No. 3, (2019), pp. 326-347.*

[18] A. Sur and M. Kanoria, “Field equations and corresponding memory responses for a fiber-reinforced functionally graded due to heat source”, *Mech.*, *vol.* ***49****, No. 4, (2019), pp. 511-533.*

[19] A. Sur, S. Santra and M. Kanoria, “Memory response on thermal wave propagation in an elastic solid with voids due to influence of magnetic field”, *Waves Random Complex Media*, *vol.* ***31****, No. 6, (2019), pp. 1187-1210.*

[20] S. Mondal, A. Sur and M. Kanoria, “Photo-thermo-elastic wave propagation under the influence of magnetic field in presence of memory responses”, *Mech.*, *vol.* ***49****, No. 6, (2021), pp. 862-883.*

[21] S. Mondal, A. Sur, D. Bhattacharya and M. Kanoria, “Thermoelastic interaction in a magneto-thermoelastic rod with memory dependent derivative due to the presence of moving heat source”, *Ind. J. Phys.*, *vol.* ***94****, (2020), pp. 1591-1602.*

[22] P. Das and M. Kanoria, “Study of finite thermal waves in a magneto-thermoelastic rotating medium”, *J. Therm. Stresses, (2014), vol.* ***37****, pp. 405-428.*

[23] A. M. Zenkour and A. Abouelregal, “Two-temperature theory for a heated semi-infinite solid by a pulsed laser radiation”, *Arch. Thermodyn.*, *vol.* ***41****, No. 2, (2020), pp. 85-101.*

[24] A. Abouelregal and A. Zenkour, “A generalized thermoelastic medium subjected to pulsed laser heating via a two-temperature model”, *JTAM*, *vol.* ***57****, No. 3, (2019), pp. 631-639.*

[25] M. Kutbi and A. Zenkour, “Thermoelastic interactions in an unbounded solid due to a continuous heat source using the modified TPL G-N model", *Waves in Random and Complex Media*, *vol.* ***32,*** *No. 3, (2020), pp. 1363-1384.*

[26] A. De, P. Purkait, P. Das and M. Kanoria, “Effect of magnetic field and inclined load on a two-Dimensional thermoelastic medium under gravity”, *MMS.*, *vol.* ***14****, No. 3, (2023).*

[27] P. Purkait and M. Kanoria, “The effect of inclined load and gravitational field on a 2-D thermoelastic medium under the influence of pulsed laser using dual phase lag model”, *Mechanics Based Design of Structures Machines*, *vol.* ***51****, No. 11, (2023), pp. 6497-6512.*

[28] D. J. Halsted and D.E. Brown, “Zakians technique for inverting Laplace transforms”, *J. Chem. Eng.*, *vol. 3, (1972), pp. 312-313.*

[29] H. M. Al-Qahtani and S.K. Datta, Laser-generated thermoelastic waves in an anisotropicinfinite plate: Exact analysis, *J. Therm. Stresses*, *vol. 31, No. 6, (2008), pp. 569-83.*

[30] M. I. A. Othman and S. Mondal, “Memory-dependent derivative effect on 2D problem of generalized thermoelastic rotating medium with Lord-Shulman”, *Ind. J.Phys.*, *vol. 94, (2020), pp. 1169-1181.*

[31] R. S. Dhaliwal and A. Singh, “Dynamic coupled thermoelasticity”, *HindustanPublishing Corporation* (1980).